INTERFACE

rsif.royalsocietypublishing.org

Research

Cite this article: Toomey MB, Collins AM, Frederiksen R, Cornwall MC, Timlin JA, Corbo JC. 2015 A complex carotenoid palette tunes avian colour vision. *J. R. Soc. Interface* **12**: 20150563.
http://dx.doi.org/10.1098/rsif.2015.0563

Received: 25 June 2015
Accepted: 14 September 2015

Subject Areas:
chemical biology

Keywords:
vision, carotenoid, hyperspectral microscopy, microspectrophotometry

Author for correspondence:
Joseph C. Corbo
e-mail: jcorbo@wustl.edu

Electronic supplementary material is available at http://dx.doi.org/10.1098/rsif.2015.0563 or via http://rsif.royalsocietypublishing.org.

THE ROYAL SOCIETY PUBLISHING

A complex carotenoid palette tunes avian colour vision

Matthew B. Toomey[1], Aaron M. Collins[2], Rikard Frederiksen[3], M. Carter Cornwall[3], Jerilyn A. Timlin[2] and Joseph C. Corbo[1]

[1]Department of Pathology and Immunology, Washington University School of Medicine, St Louis, MO 63110, USA
[2]Bioenergy and Defense Technologies, Sandia National Laboratories, Albuquerque, NM 87123, USA
[3]Department of Physiology and Biophysics, Boston University School of Medicine, Boston, MA 02118-2526, USA

MBT, 0000-0001-9184-197X; MCC, 0000-0002-0847-939X; JAT, 0000-0003-2953-1721; JCC, 0000-0002-9323-7140

The brilliantly coloured cone oil droplets of the avian retina function as long-pass cut-off filters that tune the spectral sensitivity of the photoreceptors and are hypothesized to enhance colour discrimination and improve colour constancy. Although it has long been known that these droplets are pigmented with carotenoids, their precise composition has remained uncertain owing to the technical challenges of measuring these very small, dense and highly refractile optical organelles. In this study, we integrated results from high-performance liquid chromatography, hyperspectral microscopy and microspectrophotometry to obtain a comprehensive understanding of oil droplet carotenoid pigmentation in the chicken (*Gallus gallus*). We find that each of the four carotenoid-containing droplet types consists of a complex mixture of carotenoids, with a single predominant carotenoid determining the wavelength of the spectral filtering cut-off. Consistent with previous reports, we find that the predominant carotenoid type in the oil droplets of long-wavelength-sensitive, medium-wavelength-sensitive and short-wavelength-sensitive type 2 cones are astaxanthin, zeaxanthin and galloxanthin, respectively. In addition, the oil droplet of the principal member of the double cone contains a mixture of galloxanthin and two hydroxycarotenoids (lutein and zeaxanthin). Short-wavelength-absorbing apocarotenoids are present in all of the droplet types, providing filtering of light in a region of the spectrum where filtering by hydroxy- and ketocarotenoids may be incomplete. Thus, birds rely on a complex palette of carotenoid pigments within their cone oil droplets to achieve finely tuned spectral filtering.

1. Introduction

Many bird species communicate through elaborate visual displays, and a majority of birds rely on vision as their primary sensory modality [1]. The importance of vision is reflected in the morphological complexity and functional specializations of avian photoreceptors. The avian retina contains six photoreceptor types: rods that mediate dim light vision, four spectrally distinct single cones that mediate tetrachromatic colour vision in bright light and double cone photoreceptors that are thought to contribute to luminance discrimination [2–4]. Each of the cone photoreceptor types contains a differently coloured oil droplet located within its inner segment that filters light as it passes through the cell on its way to the photosensitive outer segment [5] (figure 1*a*,*b*). This filtering narrows the spectral bandwidth of the cones and shifts their peak sensitivities in ways that are predicted to enhance colour discrimination and colour constancy [7–9].

The elegant tuning of avian spectral sensitivity relies on the precise matching of the oil droplet spectral filtering and photopigment sensitivity within each cone subtype [7,9]. Photopigment sensitivity is determined by the amino acid composition of the opsin protein, which binds an 11-*cis* retinal chromophore [10–14]. Changes in the amino acid composition of the opsin result in shifts in the spectral positioning

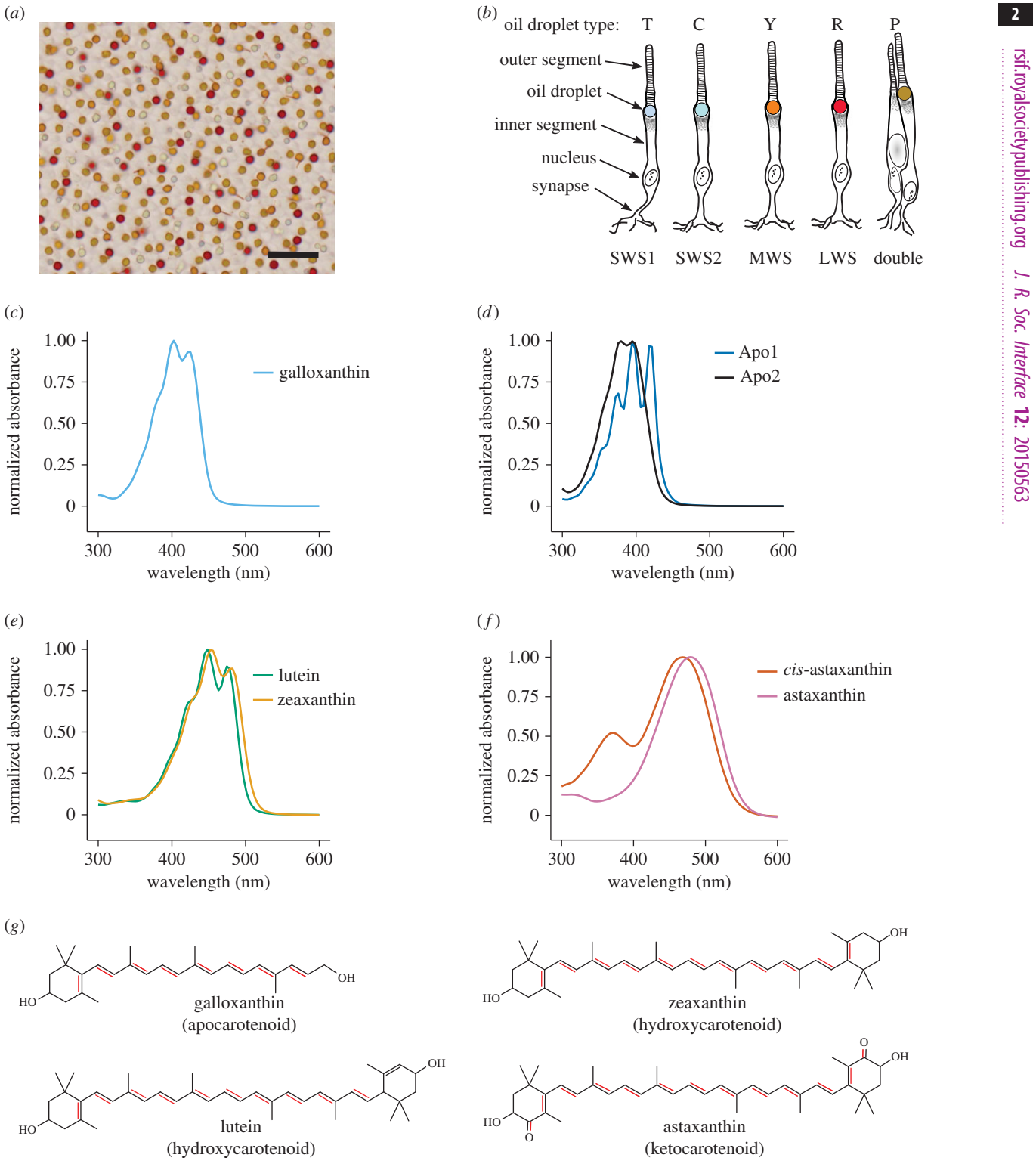

Figure 1. (*a*) Brightfield image of a flat-mounted P21 chicken retina showing the distinctive coloration of the cone oil droplets (scale bar = 10 µm). (*b*) A schematic representation of the photoreceptor subtypes of the avian retina: rods, short-wavelength sensitive type 1 (SWS1), short-wavelength sensitive type 2 (SWS2), medium-wavelength sensitive (MWS), long-wavelength sensitive (LWS), and double cones. The oil droplet is coloured to approximate its appearance in the brightfield image. Figure modified from [6]. (*c–f*) Normalized absorbance spectra of the major (*c*,*d*) apocarotenoids, (*e*) hydroxycarotenoids and (*f*) ketocarotenoids found in the avian retina. The molecular structures of representative carotenoids are shown in (*g*) with the double bonds in conjugation (highlighted in red) that contribute to the absorbance spectra.

of the photopigment peak sensitivity (λ_{max}). The complementary filtering of the cone oil droplets is achieved through the accumulation of specific types of carotenoid pigments that function as sharply defined long-pass cut-off filters [5]. The absorbance spectra of carotenoids are determined by the degree of conjugation in the molecule and can be shifted to longer or shorter wavelengths through the addition or subtraction, respectively, of conjugated double bonds [15]. Thus, at the level of the photoreceptor, spectral sensitivity is shaped by two distinct mechanisms: (i) the tuning of photopigment sensitivity through opsin sequence evolution and (ii) the precise control of the metabolism and accumulation of carotenoid pigments in the cone oil droplets. The mechanisms of opsin tuning are relatively well understood, and bird opsins

have become a model system for exploring adaptive evolution at a molecular level [12,13,16–19]. In contrast, our understanding of the carotenoid composition and spectral filtering of the cone oil droplets remains limited.

The small size, shape and high density of the cone oil droplets pose major analytical challenges. For example, direct absorbance measurements of the droplets by microspectrophotometry (MSP) are confounded by light that scatters around the droplets [20,21]. Therefore, many studies of avian visual function have relied upon simplified models of the oil droplet spectra [22–24] or assumed that the droplets are pigmented with a single pure carotenoid type [25]. However, Goldsmith *et al.* [5] indicated that some cone oil droplets contain mixtures of carotenoids, which may impact their spectral filtering function in unappreciated ways. The goal in this study was to examine this possibility by determining the precise carotenoid composition and spectral filtering of avian cone oil droplets.

Carotenoids are well known as the diet-derived pigments that create the vibrant colours of many birds, including the red of the cardinal's (*Cardinalis cardinalis*) plumage or the bright yellow of the canary's (*Serinus canaria*) feathers. Their presence in the avian retina was first suggested over a century ago [26], and the first detailed characterizations of these retinal pigments were made more than 60 years ago [27,28]. In early work, Wald and co-workers [27,28] identified four major classes of carotenoids in the avian retina that absorb light in different portions of the ultraviolet/visible spectrum, corresponding to their degree of conjugation: apocarotenoids (seven or eight conjugated double bonds), carotenes (11 conjugated double bonds), hydroxycarotenoids (11 conjugated double bonds), and ketocarotenoids (13 conjugated double bonds; figure 1*c*,*f*). Subsequently, Goldsmith *et al.* [5] inferred the carotenoid composition of individual oil droplets by matching the absorbance spectra of isolated expanded droplets to pure carotenoid spectra. They found that the transparent droplets of the short-wavelength-sensitive type 1 (SWS1) cones do not contain carotenoids, and thus have no significant absorbance at wavelengths greater than 300 nm. In contrast, the oil droplets of the long-wavelength-sensitive (LWS), medium-wavelength-sensitive (MWS) and short-wavelength-sensitive type 2 (SWS2) cones each contained a single dominant carotenoid: astaxanthin, zeaxanthin and galloxanthin, respectively. Additionally, the principal member of the double cone had a spectrum that suggested the presence of a mixture of galloxanthin and zeaxanthin [5]. While these observations indicate the dominant pigment within each cone oil droplet type, they do not reveal to what extent mixtures of carotenoids might influence the droplets' spectral filtering function.

To elucidate the carotenoid composition of avian cone oil droplets, we examined the retinas of the domestic chicken (*Gallus gallus*) using three different approaches. First, we characterized the carotenoid composition of whole retinas using high-performance liquid chromatography (HPLC), which revealed the presence of seven major carotenoid species. Next, we used hyperspectral confocal fluorescence microscopy to examine cone oil droplets *in situ* and map the distribution of carotenoids among the cone photoreceptor types. This analysis revealed that the oil droplets contain a more complex mixture of carotenoids than previously thought. Lastly, we used MSP to measure detailed light absorbance spectra from intact and diluted cone oil droplets and estimated the composition of individual droplet types by fitting these complex spectra with mixtures of the pure carotenoid spectra from the palette of pigments we identified in our HPLC analyses.

2. Material and methods

2.1. Sample collection

Retinas were collected from 21 day old white leghorn chickens (*G. gallus*) hatched from fertilized specific pathogen-free eggs purchased from Charles River Laboratories (North Franklin, CT) and reared on a carotenoid-rich diet (Start & Grow; Purina Mills, St Louis, MO). The birds were euthanized by carbon dioxide asphyxiation following an approved protocol (Washington University ASC protocol no. 20140072), the eyes were dissected, and the retinas were processed as described below.

2.2. Chromatographic analysis of retinal carotenoid content

HPLC was used to identify and quantify the carotenoid composition of whole retinas. Immediately after harvest, retinas were frozen at −80°C and stored for up to four months prior to analysis. We thawed the retinas on ice, added 500 µl of phosphate-buffered saline (PBS) and homogenized them on ice using a glass dounce homogenizer. We measured the total protein content of the homogenate with a bicinchoninic acid assay following the manufacturer's instructions (cat. no. 23250; Thermo Scientific, Rockford, IL). Five hundred microlitres of the retinal homogenate was transferred to a 9 ml glass culture tube and extracted three times with 500 µl of hexane : *tert*-butyl methyl ether 1 : 1 (vol. : vol.). The extracted material was split equally between two tubes, and dried under a stream of nitrogen. The extracts were saponified with 1 ml of 0.02 M NaOH in methanol for 4 h or 0.2 M NaOH for 6 h, under nitrogen, at room temperature in the dark. The two different saponification conditions are optimized for the recovery of ketocarotenoids (0.02 M NaOH) or hydroxycarotenoids, carotenes and apocarotenoids (0.2 M NaOH) [29]. Saponification is necessary because the carotenoids in the avian retina occur as fatty acid esters that must be removed before HPLC analysis [29]. Following incubation in the dark, the reaction was stopped with the addition of 1 ml of saturated NaCl in water, then 2 ml of water. The saponified carotenoids were extracted with 2 ml of hexane : *tert*-butyl methyl ether 1 : 1 (vol. : vol.) and then dried under a stream of nitrogen.

For HPLC analysis, the dried saponified samples were resuspended in 200 µl of methanol : acetonitrile 1 : 1 (vol. : vol.), and 100 µl was injected into an Agilent 1100 series HPLC machine fitted with a reverse-phase YMC carotenoid 5.0 µm column (4.6 × 250 mm). The samples were monitored with a UV/Vis diode array detector at 350, 400, 445 and 480 nm and eluted using two different HPLC methods, as detailed in electronic supplementary material, table S1. We used method A to separate and quantify the ketocarotenoid samples and method B for the apocarotenoids, hydroxycarotenoids and carotene samples. Carotenoids were identified and quantified by comparison with authentic standards that were gifts of DSM Nutritional Products (Parsippany, NJ) or purchased from CaroteNature GmbH (Ostermundigen, Switzerland).

2.3. Hyperspectral confocal fluorescence microscopy

A custom-built hyperspectral confocal microscope [30] was used to acquire detailed spectrally resolved images of the laser-stimulated fluorescence and resonance-enhanced Raman scattering of the carotenoids within the cone oil droplets. Freshly dissected chicken retinas were fixed overnight in 4% paraformaldehyde, washed

Table 1. Major carotenoid peaks observed in HPLC analysis of 21 day old chicken retinas ($n = 3$). The major λ_{max} values of the absorbance spectra are given in italics and parentheses denote shoulders in the spectrum. The concentration is given as μg per mg of protein.

carotenoid	R_t (min)	λ_{max} (nm)	concentration (μg mg^{-1})	% of total
apocarotenoids				*46.0*
Apo1	5.6	375, *396*, 420	0.207 ± 0.053	10.3
Apo2	5.9	(356), *380*, 396	0.208 ± 0.079	10.3
galloxanthin[a]	7.1	(380), *402*, 424	0.511 ± 0.169	24.4
ketocarotenoids				*26.4*
cis-astaxanthin[a]	6.9	372, *468*	0.093 ± 0.015	4.6
astaxanthin[a]	7.7	*479*	0.366 ± 0.044	18.2
hydroxycarotenoids				*24.4*
lutein[a]	18.4	(424), *448*, 476	0.153 ± 0.056	7.6
zeaxanthin[a]	23.4	(426), *453*, 480	0.155 ± 0.065	7.7

[a]Carotenoids identified by comparison with authentic standards.

with PBS and then mounted photoreceptor side up on a microscope slide in 20% glycerol in PBS. Samples were shipped overnight from the collection site (Washington University, St Louis, MO) to the microscopy laboratory (Sandia National Laboratory, Albuquerque, NM) and analysed within 48 h of being collected. The samples were kept on ice and protected from light throughout preparation and shipping to limit degradation of the carotenoids. Reference carotenoids were collected from purified HPLC fractions of chicken retina ($n = 10$, P21) as described above. We dissolved 0.8–16.4 μg of each carotenoid in 0.25 mg of glyceryl trilinoleate (T9517; Sigma, St Louis, MO), suspended the carotenoid/lipid droplets in PBS, and spotted them onto microscope slides for analysis.

The general hyperspectral microscopy methodology has been described previously [30,31]. Briefly, a 488 nm laser was focused onto the sample through a 60× (1.4 numerical aperture) apochromat objective. Raman scatter and fluorescent emission (500–800 nm) were collected at a resolution of 3 nm by the same objective and spectrally dispersed through a custom-built prism spectrometer onto an electron multiplied CCD camera. Images were 25 × 25 μm and acquired at 240 μs per voxel (spatial resolution: 240 × 240 × 600 nm). In some instances, successive images were acquired at an axial spacing of 1 μm to acquire spectral data from cone oil droplets at various depths in the retina. Following pre-processing as described previously [32], spectral images were combined into a composite spectral image dataset and were analysed with custom multivariate curve resolution (MCR) algorithms [33–35] as described previously [31,36] (and references therein) to identify component spectral signatures.

From the MCR processing of the hyperspectral fluorescence and Raman images, we obtained image stacks, with each slice representing the mean intensity along the *z*-axis for a given spectral component. The droplets were then identified, and the component intensities were measured from the stacks using ImageJ [37]. To group the droplets by composition of their emission spectra, we used the partitioning around medoids (PAMs) method [38]. The PAM analysis was implemented in R v. 3.1.3 [39] using the cluster package [40]. We found that clustering the droplets into four groups provided the best fit to the data and maximized the average silhouette width coefficient (mean $s_i > 0.68$), a measure of clustering quality [41].

2.4. Expanded oil droplet microspectrophotometry

Owing to the high pigment density and refractive index (RI) of the cone oil droplets, it is not possible to collect detailed absorbance spectrum measurements with conventional MSP approaches [5,20]. To overcome these limitations, we used the methods of Liebman & Granda [20] to dilute the pigment and reduce the RI of the droplets by expanding them with mineral oil. Freshly dissected retinas were lysed in 1 ml distilled water by trituration and vortexing, and then centrifuged at 10 000*g* for 2 min in a tabletop centrifuge. The oil droplets were collected from the surface of the liquid and transferred to a new tube containing 500 μl of distilled water. The oil droplet/water mixture was spotted onto concanavalin A (C5275; Sigma)-coated quartz coverslips and dried by incubating at 50°C for 10 min. To reduce potentially confounding light scatter, we covered the dried droplets with glycerol (G5516; Sigma), which has an RI (approx. 1.471) similar to that of the mineral oil (RI ~ 1.476). The light absorbance spectra of the oil droplets were measured with a custom-built microspectrophotometer described previously [42]. Isolated droplets were scanned from 350 to 700 nm, and the droplet diameter was measured both before and after expansion with mineral oil. The droplets were then expanded by fusing them with a droplet of light mineral oil (330779; Sigma) expressed from the tip of a pulled glass pipette. We calculated the peak optical density (OD) of the unexpanded droplets following Goldsmith *et al.* [5].

2.5. Fitting oil droplet spectra with pure carotenoid spectra

To estimate the carotenoid composition of the cone oil droplets, we used a linear additive model to find the combination of pure carotenoid spectra that best fit the measured oil droplet spectra. The absorbance spectra from 350 to 700 nm of the seven major carotenoids observed in the HPLC analyses of whole retinas (table 1) were normalized to a peak absorbance value of 1 (figure 1*c*). Then, nonlinear least-squares (nls) regression in the base package of R v. 3.1.3 [39] was used to fit these pure carotenoid spectra to the normalized absorbance spectra of the expanded oil droplets with the following model:

$$D_{\text{oildroplet}}(\lambda) = a_{\text{apo1}}D_{\text{apo1}}(\lambda) + a_{\text{apo2}}D_{\text{apo2}}(\lambda) + a_{\text{gal}}D_{\text{gal}}(\lambda) + a_{\text{asta}}D_{\text{asta}}(\lambda) + a_{c-\text{asta}}D_{c-\text{asta}}(\lambda) + a_{\text{lut}}D_{\text{lut}}(\lambda) + a_{\text{zea}}D_{\text{zea}}(\lambda),$$

where D is the normalized spectrum of the respective pure carotenoids or the spectrum of the oil droplet to be fitted at the wavelength λ, and a is the relative density of each pure carotenoid. We used the 'port' algorithm to find the best fit values for a,

constraining a to values ≥ 0, and set the starting values of a to 0. To ensure that the models converged to global minima, the mean expanded droplet spectra were fitted with all possible initial a values from 0 to 1, incremented by 0.2, using the 'brute-force' method in the nls2 package [43]. The starting points identified with this method and starting values of 0 for all a values converged to identical values (electronic supplementary material, table S2).

2.6. Spectral filtering of pure and mixed carotenoid droplets

To examine the impact of carotenoid mixing on the spectral filtering function of the cone oil droplets, we predicted and compared the spectra of the measured oil droplets and pure carotenoids over a range of optical densities. We calculated absorptance spectra following Goldsmith & Butler [44]:

$$A(\lambda) = 1 - 10^{aD(\lambda)},$$

where a is the peak OD of the droplet and D is the normalized droplet or pure carotenoid spectrum. We predicted the spectra for a range of optical densities ($a = 0.1–12.5$) and calculated the cut-off wavelengths (λ_{cut}) from these spectra following a published method [21]. λ_{cut} provides a measure of the spectral location of the long-pass filtering of the droplet and is defined as the wavelength at the intersection of the tangent to the long-wavelength limb of the absorbance curve and the maximum absorbance of the droplet [21]. We also calculated the proportion of short-wavelength light transmitted by these spectra as the average of transmittance $1 - A(\lambda)$ from 350 to 400 nm.

3. Results

3.1. Chromatographic analysis of retinal carotenoid content

In our initial analysis, we sought to determine the palette of carotenoid pigments present in the avian retina using HPLC. We identified seven major species of carotenoid (each constituting greater than 2% of total) in the post-hatch day 21 (P21) chicken retina. These seven carotenoid types fall into four major classes. The most abundant class was the apocarotenoids, making up 46% of the total carotenoid content of the retina (table 1). Apocarotenoids are the product of an oxidative cleavage of C40 carotenoids [45], which produces a relatively truncated system of conjugated double bonds and short-wavelength shifted absorbance spectra (figure 1*c*,*d* and table 1). The most abundant member of this class was galloxanthin with eight conjugated double bonds. We also observed two other apocarotenoids (Apo1 and Apo2), whose structures are currently unknown. Apo1 has an absorbance peak similar to galloxanthin (396 nm) but a more sharply peaked absorbance spectrum (figure 1*d*), which is characteristic of carotenoids containing an ε-ring configuration [46]. Apo2 has a fine structure similar to that of galloxanthin, but is short-wavelength shifted by 22 nm (figure 1*d*).

The second most abundant class of carotenoids in the chicken retina was the ketocarotenoids, making up 26.4% of total carotenoid content. This group has ketone functional groups in the 4 and 4′ positions that extend the conjugated system, thereby producing a long-wavelength absorbance spectrum with a single broad peak (figure 1*f*). The most abundant members of this group were *cis* and *trans* isomers of astaxanthin (table 1). We also observed two minor ketocarotenoid peaks in our HPLC analyses, but these each made up less than 2% of the total carotenoid profile and were not included in our subsequent fitting analyses (electronic supplementary material, table S4 and figure S5).

Hydroxycarotenoids made up 24.4% of the total carotenoid content of the chicken retina. Hydroxycarotenoids are characterized by hydroxyl functional groups in the 3 and 3′ positions of the β-ionone ring, which increase the polarity of the molecule but do not have a major influence on their spectral absorbance (figure 1*e*). The most abundant members of this group were lutein and zeaxanthin (table 1). We also observed five minor hydroxycarotenoid peaks in our HPLC analyses; however, each made up less than 1.5% of the total carotenoid profile (electronic supplementary material, table S4 and figure S5).

Lastly, we observed small amounts (3% of total) of a single carotene in the chicken retina that we have putatively identified as ε,ε′-carotene, based on published descriptions [5] (electronic supplementary material, table S4 and figure S5).

3.2. Hyperspectral microscopy of oil droplets

Having determined the palette of carotenoid pigments present in the chicken retina, we next sought to determine the distribution of these carotenoids among the cone oil droplets using hyperspectral microscopy. Spectrally resolved fluorescence and Raman scatter were collected on a total of 213 individual pigmented oil droplets from the central and mid-peripheral retina of the chicken. We also observed a subset of oil droplets by bright field microscopy that did not produce detectable emission and are consistent with the unpigmented T-type droplets of the SWS1 cones. Among the other oil droplet classes, several carotenoid Raman vibrations were resonance enhanced by the excitation laser (488 nm) producing emission spectra with Raman bands superimposed on a broad fluorescence signal (figure 2*b–e*) [30]. Without any prior information regarding the known spectra of carotenoids, we derived four components from de novo MCR processing of the oil droplet spectra that explained greater than 99% of the spectral variation and were closely matched to the spectra of the major carotenoids found in the avian retina (figure 2*b–e*). Subtle differences between the oil droplet spectral components and the authentic standards are likely to reflect differences in the solvent environment of the droplets and standards [47]. The intensity of the emission spectra generated by a given amount of purified carotenoid varied by as much as 20-fold among the carotenoid types (figure 2*f*), indicating that signal intensity is not a direct measure of abundance.

We observed all four MCR spectral components in nearly every droplet we analysed, and the relative intensity of the components varied among the oil droplets. Therefore, we could readily assign each oil droplet to one of four distinct groups by PAM clustering analysis of the relative spectral component intensities (figure 3*a*). Group 1 was the largest with 125 droplets (58.6% of total), and all four components contributed similar proportions to the spectra of this group (figure 3*a*,*b*). Group 1 most likely comprises P-type droplets of the double cone, which are the most abundant class in the retina [6] and were previously postulated to have a mixed carotenoid composition [5]. Group 2 contained 32 droplets (15.0% of total), with spectra dominated by hydroxycarotenoid components (c1 and c2). The frequency

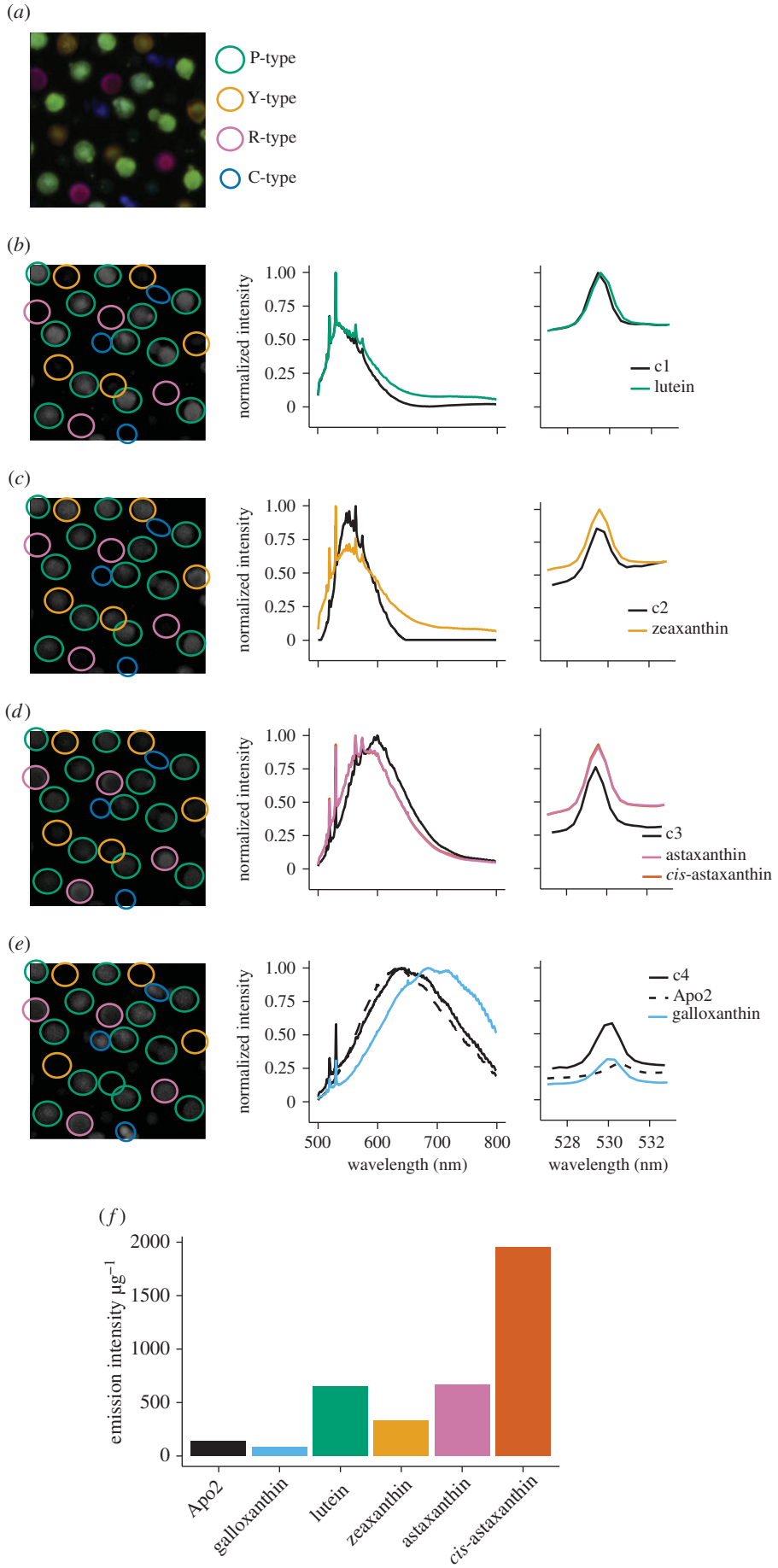

Figure 2. (*a*) False colour composite image of the cone oil droplets showing the relative contributions of the four spectral components to the droplet emission spectra, as measured by hyperspectral fluorescence microscopy and defined by MCR analysis. (*b–e*) The multivariate curve resolution (MCR) spectral components derived from the cone oil droplet emission spectra overlaid with the best matched emission spectra of the pure preparations of the major carotenoids in the avian retina. Right: detailed view of the major resonance peak. (*f*) The peak emission intensity per microgram of the pure carotenoid preparations.

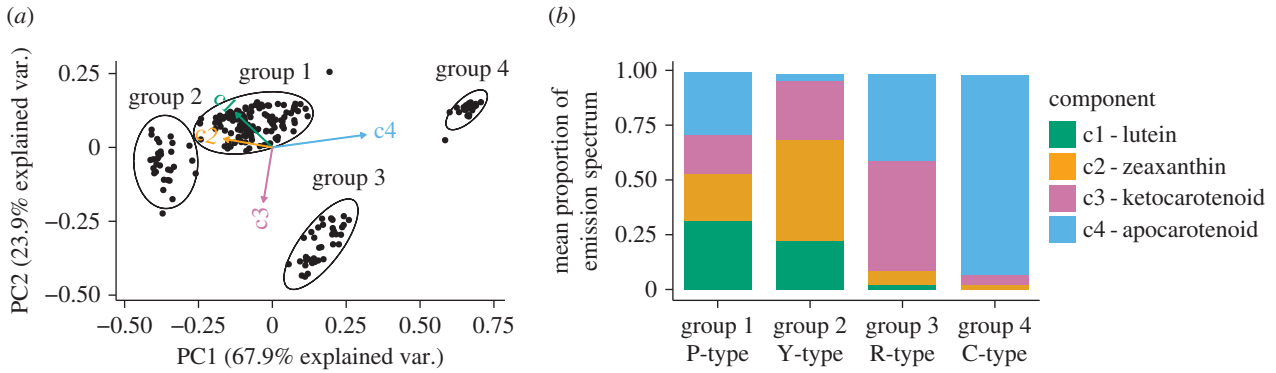

Figure 3. (*a*) Oil droplet groupings identified by the PAM clustering analysis of the relative intensity of the four MCR components of the emission spectra. The *x*- and *y*-axes are principal components (PC) 1 and 2 derived from the MCR spectral components. The contributions of these components are represented by the arrows superimposed on the plot. (*b*) A stacked bar chart shows the mean relative intensity of the four MCR components of the emission spectra within each of the droplet groups.

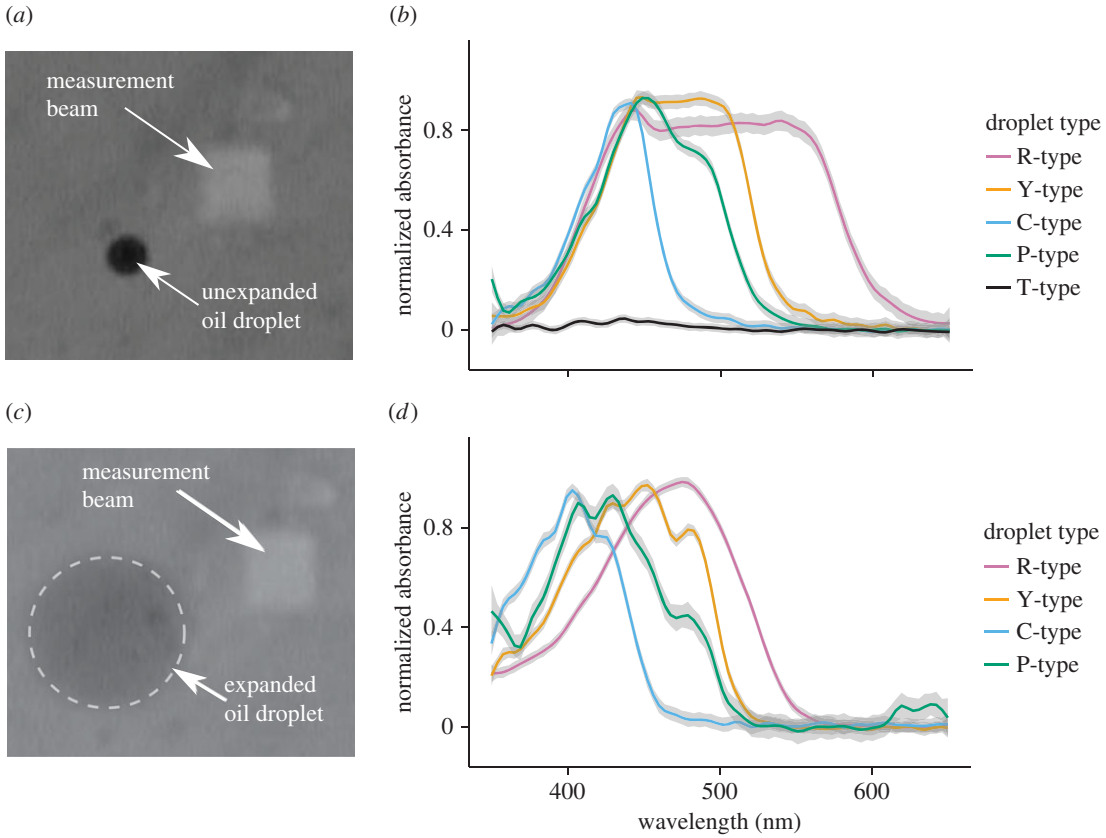

Figure 4. (*a*) An unexpanded R-type droplet imaged through the MSP system. The measurement beam is located to the right of the droplet. (*b*) The mean normalized absorbance spectra of the unexpanded oil droplets measured with the beam MSP. The standard error of the mean is shown as the grey interval around each line. The apparent transmission at short wavelengths is an artefact of light scattering around the optically dense droplets. (*c*) The same droplet shown in (*a*) after expansion with mineral oil. (*d*) The mean $\pm$ s.e. normalized absorbance spectra of the oil droplets after expansion with mineral oil.

and composition of these droplets are consistent with the Y-type oil droplet of the MWS cone (figure 3*a*,*b*). Group 3 contained 35 droplets (16.4% of total), with spectra containing a large ketocarotenoid component (c3) consistent with R-type droplets (figure 3*a*,*b*) of the LWS cone. Group 4 contained 21 droplets (9.9% of total), with apocarotenoid-dominated spectra consistent with C-type droplets (figure 3*a*,*b*) of the SWS2. The frequencies of oil droplet types identified in this analysis are comparable to those observed in previous studies [6] and, taken together, these results indicate that all of the droplets contain complex mixtures of carotenoids. However, variation in the sensitivity of the hyperspectral analyses to the different carotenoids limits our ability to estimate the precise abundance of each type in individual oil droplets.

3.3. Expanded oil droplet microspectrophotometry

Next, we used MSP to determine the relative concentration of the carotenoids within each oil droplet type. We acquired detailed absorbance spectra by diluting and expanding isolated droplets following published methods [5,20] (figure 4*a*,*c*). We measured the absorbance spectrum and droplet diameter before and after expansion for a total of 19 pigmented oil droplets and classified the droplets by the cut-off wavelengths (λ_{cut}) of their unexpanded spectra. We

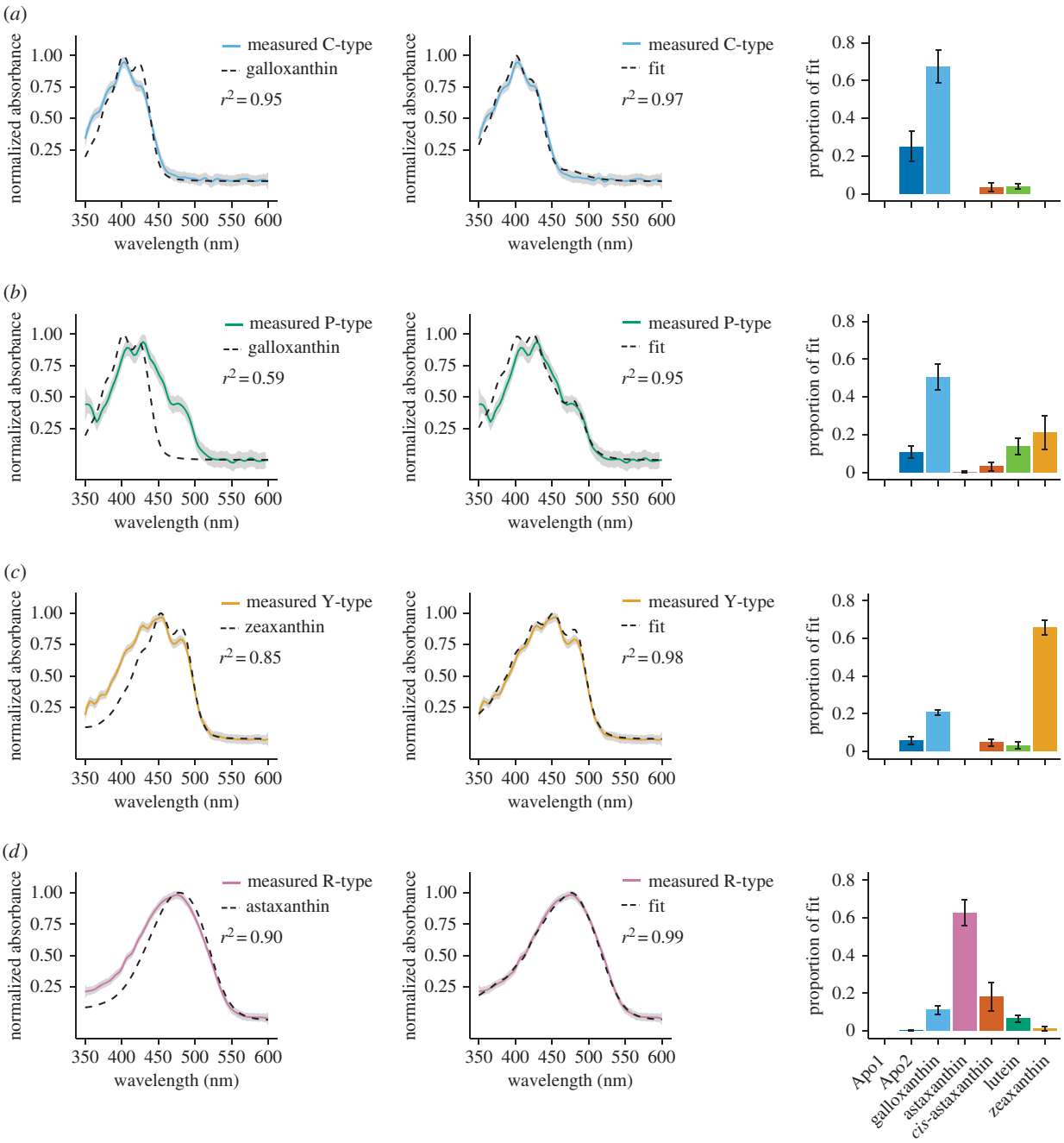

Figure 5. The pure (left) or mixed (middle) carotenoid spectra that best fit the spectra of expanded (*a*) C-type, (*b*) P-type, (*c*) Y-type and (*d*) R-type oil droplets. The mean ± s.e. proportion of each carotenoid type in the mixed carotenoid fit (middle) is shown in the bar graphs to the right of each curve.

identified four classes of pigmented droplets, R-type ($n = 5$, $\lambda_{cut} = 543.5 \pm 11.8$ nm), Y-type ($n = 4$, $\lambda_{cut} = 496.9 \pm 5.8$ nm), C-type ($n = 5$, $\lambda_{cut} = 438 \pm 1.0$ nm) and P-type ($n = 5$, $\lambda_{cut} = 449.1 \pm 7.5$ nm; figure 4*b*) droplets. These cut-off values are consistent with the ranges previously reported for chickens [48]. The unexpanded droplets had relatively structureless cut-off absorbance spectra, similar to those previously reported (figure 4*b*) [49]. There was significant transmittance in the droplets at short wavelengths (less than 400 nm), but this was an artefact probably caused by scattering of the measurement beam [21]. In contrast, our measurement of expanded droplets produced well-resolved complex spectra (figure 4*d*). OD differed significantly among the cone oil droplet types ($F_{3,15} = 25.42$, $p < 0.001$). The R-type droplets were the most dense (OD $= 11.3 \pm 1.6$), followed by the Y-type droplets (5.0 ± 0.3), then the C-type droplets (2.4 ± 0.4). P-type droplets were the least dense (1.5 ± 0.4).

We estimated the pigment composition of the droplets by fitting mixtures of pure carotenoid spectra to the expanded oil droplet spectra. To validate this approach, we measured mixtures of known carotenoid composition and fitted them with the pure spectra as detailed above (§2.5). We found that this curve-fitting method yielded highly accurate estimates of the carotenoid content (electronic supplementary material, S5. Spectral curve-fitting validation).

Next, we analysed the expanded cone oil droplets. The C-, Y- and R-type droplet spectra were dominated by a single carotenoid type and fitting these with pure galloxanthin, zeaxanthin and astaxanthin, respectively, explained the majority of variation (figure 5*a*,*c*,*d*). However, adding additional carotenoid types to the analysis substantially improved the fit to the spectra and explained as much as 99% of variation in some types (figure 5*a*,*c*,*d*). The spectra of the P-type droplets were best fitted by galloxanthin with significant contributions from hydroxycarotenoids (figure 5*b*).

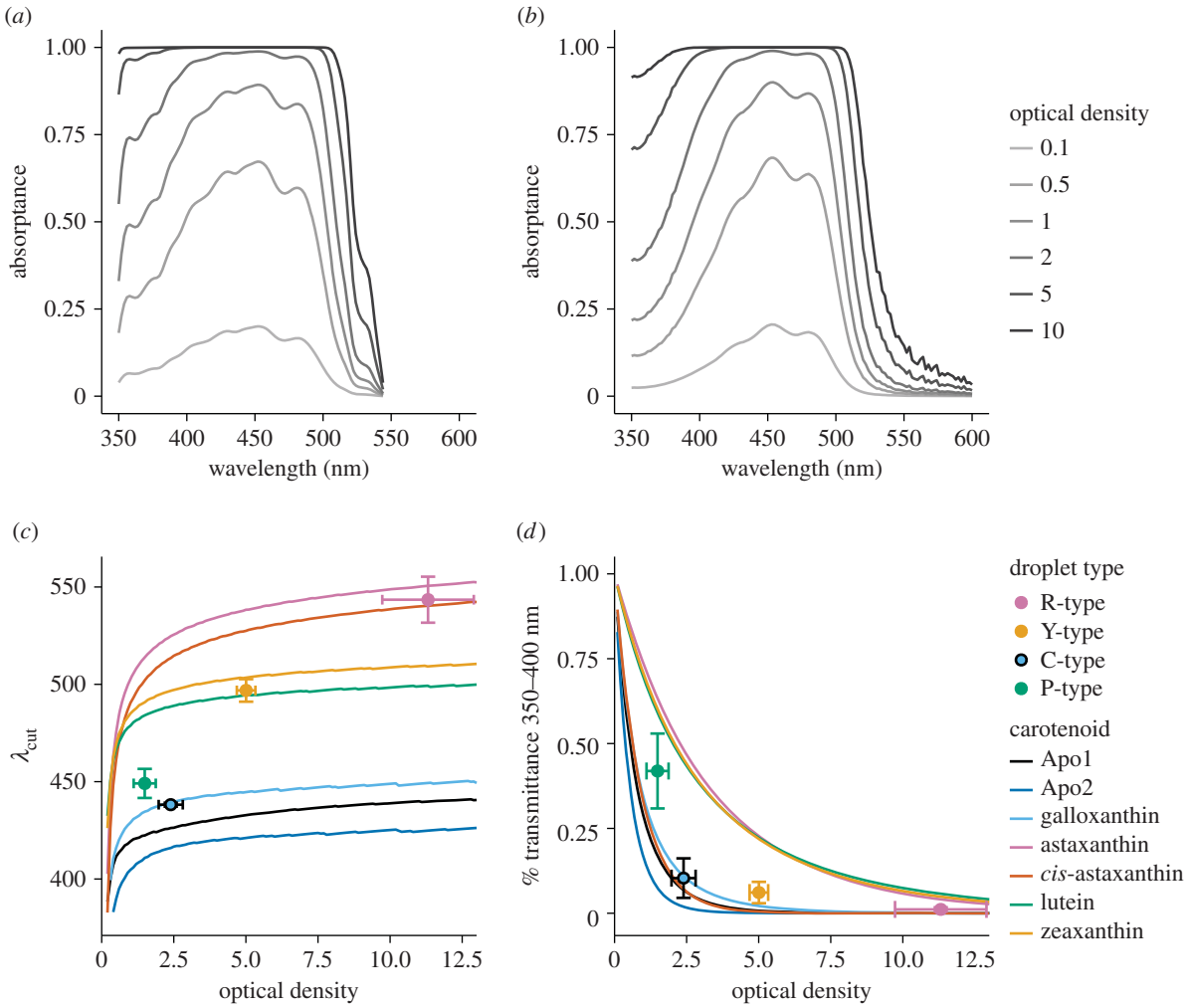

Figure 6. An example of the absorptance spectra over a range of optical densities calculated from (*a*) the expanded Y-type droplet spectrum and (*b*) the pure zeaxanthin spectrum. These calculated spectra were used to predict λ_{cut} and short-wavelength transmittance of the pure carotenoids over a range of optical densities. (*c*) The measured mean $\pm$ s.e. of λ_{cut} and optical density (OD) of the cone oil droplets (points) overlaid on the λ_{cut} predicted for pure carotenoid spectra over a range of optical densities. (*d*) The measured mean $\pm$ s.e. short-wavelength (350–400 nm) transmittance and OD of the cone oil droplets (points) overlaid on the short-wavelength transmittance predicted for pure carotenoid spectra over a range of optical densities.

Overall, these results agree with our hyperspectral confocal microscopy analysis indicating a complex mixture of carotenoids within each of the cone oil droplet types and support the previously hypothesized identities of the dominant pigments within each droplet type [5].

3.4. Spectral filtering of pure and mixed carotenoid droplets

To examine how the mixture of carotenoids and their concentrations contribute to the spectral filtering function of the cone oil droplets, we compared long-wavelength filtering cut-off (λ_{cut}) and short-wavelength (350–400 nm) transmittance of the measured droplets to hypothetical droplets containing a single pure carotenoid type over a range of optical densities (figure 6*a*,*b*). The predicted λ_{cut} for each of the pure carotenoids rises rapidly as the OD increases from zero, but then plateaus at high optical densities (figure 6*c*). The rate of change in the predicted λ_{cut} value varies among the different carotenoid types. For example, the λ_{cut} predicted for the apocarotenoid galloxanthin increases by 4.3 nm as the OD increases from 5 to 10, and the λ_{cut} predicted for zeaxanthin changes by 5.3 nm over the same range. In contrast, the predicted λ_{cut} of astaxanthin increases by 10.5 nm over this range. Thus, the degree to which λ_{cut} can be tuned through changes in concentration differs among the different carotenoid types.

The measured λ_{cut} of the R-, Y- and C-type droplets were well matched by the predictions from pure astaxanthin, zeaxanthin and galloxanthin droplets, respectively, at comparable optical densities (figure 6*c*). The λ_{cut} of the P-type droplets was not well matched by the predictions for any of the pure carotenoid spectra. This is likely to reflect the low OD of the P-type droplets and the combined spectral contributions of the short-wavelength-absorbing apocarotenoids and long-wavelength-absorbing lutein and zeaxanthin. The measured short-wavelength transmittance of all of the single cone oil droplets was very low, and the transmittance of the Y-type droplets was significantly lower than the values predicted from the spectrum of pure zeaxanthin alone ($t_3 = -4.1$, $p = 0.026$, figure 6*d*). This result suggests that the minor components, especially apocarotenoids, contribute significantly to the short-wavelength filtering function of these droplets. The transmittance of the P-type droplet was the highest among the oil droplet types and reflects the relatively low pigment density in this class of droplets. Taken together, our results indicate that the long-wavelength filtering of the single cone oil droplets is determined by the dominant carotenoid in the

droplet, but the minor components may enhance the filtering in the short-wavelength region to bring them closer to functioning as ideal long-pass filters.

4. Discussion

Carotenoid pigmented cone oil droplets play an essential role in bird vision [7–9,44], and here we provide the most detailed account of their composition to date. Consistent with previous studies [5], we identified the dominant pigment in the R-type droplet as a ketocarotenoid (astaxanthin). The primary carotenoid of the Y-type droplet was a hydroxycarotenoid (zeaxanthin), whereas apocarotenoids (e.g. galloxanthin) were the major pigments in the P- and C-type droplets. In addition, our analyses revealed that the composition of the droplets is much more complex than previously thought and that each class of oil droplets contains multiple carotenoid types. Our study also demonstrates the utility of hyperspectral microscopy and spectral curve-fitting analyses for investigating the carotenoid composition in animal tissue.

4.1. Apocarotenoids are abundant and widely distributed in avian cone oil droplets

The apocarotenoid galloxanthin was among the most abundant carotenoids in the eye and was found in all four classes of pigmented oil droplets. This abundance may reflect galloxanthin's importance as a short-wavelength filter (discussed below). We also observed a second apocarotenoid (Apo2) with a short-wavelength shifted spectrum that was an important component of the C-type droplet. Apo2 is consistent with an apocarotenoid previously identified as 'fringillixanthin' in the retinas of some songbird species [5]. This molecule was hypothesized to be a truncated form of galloxanthin with seven conjugated double bonds. However, the precise structure of this molecule is currently unknown. The P-type droplets of the double cones were primarily pigmented with galloxanthin, but with large contributions from hydroxycarotenoids. This mixture produces droplets with a strong absorbance peak in UV and a weaker shoulder or peak at longer wavelengths. The long-wavelength absorbance of the P-type droplets is known to vary along the dorsal ventral axis of the eye [48,50] and probably reflects changes in the abundance of hydroxycarotenoids. Our MSP sample size was not large enough to characterize this variation; however, our hyperspectral measurements suggest considerable variation in the hydroxycarotenoid composition of the P-type droplets. The density of the P-type droplet is relatively low and is therefore unlikely to function as a sharply defined cut-off filter. These differences in density and filtering may reflect the functional specializations of the double cone discussed below.

4.2. Functional implications of complex carotenoid composition

The spectral filtering of the oil droplets of the single cone receptors is predicted to improve avian colour discrimination [7–9], and is a direct function of the types and concentrations of carotenoids within the droplets. We have found that the long-wavelength cut-off (λ_{cut}) of spectral filtering is almost wholly determined by the dominant carotenoid within each class of droplets. The experimentally measured λ_{cut} values of the single cone oil droplets were well predicted by a simple calculation of the absorptance spectra of the dominant carotenoid within each class at the measured OD of the droplet. Therefore, the complex mixtures of carotenoids in the droplets do not contribute significantly to long-wavelength filtering. Our modelling also revealed that the λ_{cut} for the pure carotenoid spectra tends to rise and then plateau as the OD increases. For most carotenoid types, there is only a small change in λ_{cut} as OD increases beyond 5. Therefore, increases in the carotenoid concentration beyond these levels may have little effect on the positioning of the spectral filtering cut-off. However, the predicted λ_{cut} of astaxanthin continues to increase at a relatively greater rate as OD increases, when compared with the other carotenoid types. Thus, there may be a greater dynamic range for tuning λ_{cut} by modulating carotenoid density in red cone oil droplets. This finding may explain the extremely high OD reported in red cone oil droplets of some birds and turtles [5,20].

The levelling off of λ_{cut} with increasing OD generates relatively discrete and predictable spectral filtering cut-offs. Therefore, a particular λ_{cut} may only be achieved by a specific combination of carotenoid types. Major shifts in the filtering of the cone oil droplets may therefore require a change in the dominant carotenoid type within the droplet. We hypothesize that carotenoid-metabolizing enzymes within individual cone types play a key role in determining the carotenoid constitution of individual oil droplet types. The plateauing of λ_{cut} at high OD may also explain why diet-driven changes in total retinal carotenoid accumulation appear to have limited impact on visually guided behaviours [51,52]. It is unlikely that relatively small changes in carotenoid concentration of already very dense single cone droplets will substantially alter the long-wavelength spectral filtering of the droplets. However, the case may be different for the low-density P-type droplets: dietary [53] or developmental light environment-induced changes [48] could impact visual function of these droplets because they are not functioning as strict cut-off filters.

The complex carotenoid mixtures in cone oil droplets contribute significantly to the short-wavelength filtering of the oil droplets. The short-wavelength transmission (350–400 nm) calculated from the measured spectra of the Y-type droplets was significantly lower than the values predicted for the pure spectra of the dominant carotenoid, zeaxanthin. Thus, the addition of short-wavelength-absorbing apocarotenoids to the dominant hydroxycarotenoids in the Y-type droplets allows them to effectively filter light ranging from the UV (less than or equal to 350 nm) up to approximately 500 nm. Vertebrate photopigments typically have two absorbance peaks, a major α-peak and a secondary β-peak in the UV [54,55]. In birds, the ocular medium is often transparent to UV [56], allowing for UV sensitivity via the SWS1 cones. However, this transmitted UV light will also stimulate the β-peak of the longer-wavelength opsins (e.g. MWS, LWS), which would compromise colour discrimination. Therefore, the short-wavelength filtering of the apocarotenoids may be an adaptation to selectively block short-wavelength light within specific subtypes of photoreceptors while allowing UV sensitivity in others.

Short-wavelength light is prone to chromatic aberration within the eye, which compromises spatial resolution [57]. This may explain why the double cones have low-density short-wavelength-absorbing apocarotenoid pigments in their droplets. The double cones are thought to primarily mediate luminance discrimination and spatial vision

[2–4,58]. Reduction of light capture with a filtering pigment seems contrary to this function. However, the cost of reduced sensitivity may be outweighed by the benefit of filtering out short-wavelength light blurred by scattering and chromatic aberration. The presence of short-wavelength-filtering apocarotenoids in pigmented droplets may also serve to protect the photoreceptors against the photooxidative effects of short-wavelength light.

Among bird species, the UV transmittance of the ocular media [56] and exposure to UV can vary widely. These variations are potentially complemented by changes in the apocarotenoid composition of the cone oil droplets. In species with UV absorptive ocular media or limited exposure to UV, we might expect relatively low levels of apocarotenoid pigmentation, while species with UV transparent media in UV-rich environments may have higher levels and a greater diversity of short-wavelength-absorbing apocarotenoids. The potential exists for a complex coevolutionary relationship between oil droplet pigmentation, ocular media transmittance and opsin spectral tuning that allows birds to fine tune their visual systems in ways we are only beginning to appreciate.

Authors' contributions. M.B.T. and J.C.C. conducted HPLC analyses, data analysis and manuscript preparation at Washington University in St Louis. M.B.T., R.F. and M.C.C. performed MSP analyses at Boston University. J.A.T. and A.M.C. carried out hyperspectral microscopy and MCR analysis at Sandia National Laboratories.

Competing interests. The authors declare no competing financial interest.

Funding. M.B.T. and J.C.C. were funded in part by Human Frontiers in Science Programme grant no. RGP0017/2011 and National Institutes of Health grant nos. RO1-EY018826 and RO1-EY024958. M.B.T. was supported by fellowships from the National Science Foundation (award no. 1202776), National Institutes of Health (5T32-EY013360-12) and the McDonnell Center for Cellular and Molecular Neurobiology at Washington University, St Louis. R.F. and M.C.C. were supported by the National Institutes of Health (R01-EY01157-42). J.A.T. and A.M.C. were supported as part of the Photosynthetic Antenna Research Center, an Energy Frontier Research Center funded by the US Department of Energy, Office of Science, Office of Basic Energy Sciences (award number DE-SC 0001035). Sandia National Laboratories is a multi-programme laboratory that is managed and operated by Sandia Corporation, a wholly owned subsidiary of Lockheed Martin Corporation, for the US Department of Energy's National Nuclear Security Administration (contract number DE-AC04-94AL85000).

Acknowledgements. We thank Susan Shen, Connie Myers and members of the Corbo laboratory for their support and constructive comments on the manuscript. We also thank Michael Sinclair for use and maintenance of the hyperspectral confocal microscope, Howland D.T. Jones for the MCR software package, Stephen M. Anthony for the Raman despiking algorithm and Dr Alian Wang for assistance measuring Raman reference spectra.

References

1. Bennett ATD, Théry M. 2007 Avian color vision and coloration: multidisciplinary evolutionary biology. *Am. Nat*. **169**, S1–S6. (doi:10.1086/510163)
2. Hart NS. 2001 The visual ecology of avian photoreceptors. *Prog. Retin. Eye Res*. **20**, 675–703. (doi:10.1016/S1350-9462(01)00009-X)
3. Campenhausen MV, Kirschfeld K. 1998 Spectral sensitivity of the accessory optic system of the pigeon. *J. Comp. Physiol. A Sens. Neural, Behav. Physiol*. **183**, 1–6. (doi:10.1007/s003590050229)
4. Osorio D, Vorobyev M, Jones CD. 1999 Colour vision of domestic chicks. *J. Exp. Biol*. **202**, 2951–2959.
5. Goldsmith TH, Collins JS, Licht S. 1984 The cone oil droplets of avian retinas. *Vision Res*. **24**, 1661–1671. (doi:10.1016/0042-6989(84)90324-9)
6. Kram YA, Mantey S, Corbo JC. 2010 Avian cone photoreceptors tile the retina as five independent, self-organizing mosaics. *PLoS ONE* **5**, e8992. (doi:10.1371/journal.pone.0008992)
7. Goldsmith TH. 1990 Optimization, constraint, and history in the evolution of eyes. *Q. Rev. Biol*. **65**, 281–322. (doi:10.1086/416840)
8. Vorobyev M, Osorio D, Bennett ATD, Marshall NJ, Cuthill IC. 1998 Tetrachromacy, oil droplets and bird plumage colours. *J. Comp. Physiol. A Sens. Neural, Behav. Physiol*. **183**, 621–633. (doi:10.1007/s003590050286)
9. Vorobyev M. 2003 Coloured oil droplets enhance colour discrimination. *Proc. R. Soc. Lond. B* **270**, 1255–1261. (doi:10.1098/rspb.2003.2381)
10. Yokoyama S, Blow NS, Radlwimmer FB. 2000 Molecular evolution of color vision of zebra finch. *Gene* **259**, 17–24. (doi:10.1016/S0378-1119(00)00435-2)
11. Hunt DM, Carvalho LS, Cowing JA, Davies WL. 2009 Evolution and spectral tuning of visual pigments in birds and mammals. *Phil. Trans. R. Soc. B* **364**, 2941–2955. (doi:10.1098/rstb.2009.0044)
12. Carvalho LS, Cowing JA, Wilkie SE, Bowmaker JK, Hunt DM. 2007 The molecular evolution of avian ultraviolet- and violet-sensitive visual pigments. *Mol. Biol. Evol*. **24**, 1843–1852. (doi:10.1093/molbev/msm109)
13. Hart NS, Hunt DM. 2007 Avian visual pigments: characteristics, spectral tuning, and evolution. *Am. Nat*. **169**, S7–S26. (doi:10.1086/510141)
14. Yokoyama S. 2000 Molecular evolution of vertebrate visual pigments. *Prog. Retin. Eye Res*. **19**, 385–419. (doi:10.1016/S1350-9462(00)00002-1)
15. Chábera P, Fuciman M, Hříbek P, Polívka T. 2009 Effect of carotenoid structure on excited-state dynamics of carbonyl carotenoids. *Phys. Chem. Chem. Phys*. **11**, 8795–8803. (doi:10.1039/b909924g)
16. Odeen A, Hastad O, Alstrom P. 2011 Evolution of ultraviolet vision in the largest avian radiation—the passerines. *BMC Evol. Biol*. **11**, 313. (doi:10.1186/1471-2148-11-313)
17. Hauser FE, van Hazel I, Chang BSW. 2014 Spectral tuning in vertebrate short wavelength-sensitive 1 (SWS1) visual pigments: can wavelength sensitivity be inferred from sequence data? *J. Exp. Zool. B Mol. Dev. Evol*. **322**, 529–539. (doi:10.1002/jez.b.22576)
18. Van Hazel I, Sabouhanian A, Day L, Endler JA, Chang BSW. 2013 Functional characterization of spectral tuning mechanisms in the great bowerbird short-wavelength sensitive visual pigment (SWS1), and the origins of UV/violet vision in passerines and parrots. *BMC Evol. Biol*. **13**, 250. (doi:10.1186/1471-2148-13-250)
19. Bloch NI, Morrow JM, Chang BSW, Price TD. 2014 SWS2 visual pigment evolution as a test of historically contingent patterns of plumage color evolution in warblers. *Evolution* **69**, 341–356. (doi:10.1111/evo.12572)
20. Liebman PA, Granda AM. 1975 Super dense carotenoid spectra resolved in single cone oil droplets. *Nature* **253**, 370–372. (doi:10.1038/253370a0)
21. Lipetz LE. 1984 A new method for determining peak absorbance of dense pigment samples and its application to the cone oil droplets of *Emydoidea blandingii*. *Vision Res*. **24**, 597–604. (doi:10.1016/0042-6989(84)90114-7)
22. Hart NS, Vorobyev M. 2005 Modelling oil droplet absorption spectra and spectral sensitivities of bird cone photoreceptors. *J. Comp. Physiol. A, Neuroethol. Sens. Neural, Behav. Physiol*. **191**, 381–392. (doi:10.1007/s00359-004-0595-3)
23. Stoddard MC, Prum RO. 2008 Evolution of avian plumage color in a tetrahedral color space: a phylogenetic analysis of new world buntings. *Am. Nat*. **171**, 755–776. (doi:10.1086/587526)
24. Endler JA, Mielke PW. 2005 Comparing entire colour patterns as birds see them. *Biol. J. Linn. Soc*. **86**, 405–431. (doi:10.1111/j.1095-8312.2005.00540.x)
25. Stavenga DG, Wilts BD. 2014 Oil droplets of bird eyes: microlenses acting as spectral filters. *Phil. Trans. R. Soc. B* **369**, 20130041. (doi:10.1098/rstb.2013.0041)
26. Capranica S. 1877 Physiologie-chemische Untersuchungen über die farbigen Substanzen der Retina. *Arch. Physiol*. **1**, 283–296.
27. Wald G, Zussman H. 1937 Carotenoids of the chicken retina. *Nature* **140**, 197. (doi:10.1038/140197a0)

28. Wald G. 1948 Galloxanthin, a carotenoid from the chicken retina. *J. Gen. Physiol*. **31**, 377–383. (doi:10.1085/jgp.31.5.377)
29. Toomey MB, McGraw KJ. 2007 Modified saponification and HPLC methods for analyzing carotenoids from the retina of quail: implications for its use as a nonprimate model species. *Invest. Ophthalmol. Vis. Sci*. **48**, 3976–3982. (doi:10.1167/iovs.07-0208)
30. Sinclair MB, Haaland DM, Timlin JA, Jones HDT. 2006 Hyperspectral confocal microscope. *Appl. Opt*. **45**, 6283–6291. (doi:10.1364/AO.45.006283)
31. Vermaas WFJ, Timlin JA, Jones HDT, Sinclair MB, Nieman LT, Hamad SW, Melgaard DK, Haaland DM. 2008 *In vivo* hyperspectral confocal fluorescence imaging to determine pigment localization and distribution in cyanobacterial cells. *Proc. Natl Acad. Sci. USA* **105**, 4050–4055. (doi:10.1073/pnas.0708090105)
32. Jones HDT, Haaland DM, Sinclair MB, Melgaard DK, Collins AM, Timlin JA. 2012 Preprocessing strategies to improve MCR analyses of hyperspectral images. *Chemom. Intell. Lab. Syst*. **117**, 149–158. (doi:10.1016/j.chemolab.2012.01.011)
33. Schoonover JR, Marx R, Zhang SL. 2003 Multivariate curve resolution in the analysis of vibrational spectroscopy data files. *Appl. Spectrosc*. **57**, 154A–170A. (doi:10.1366/000370203321666461)
34. Tauler R. 1995 Multivariate curve resolution applied to second order data. *Chemom. Intell. Lab. Syst*. **30**, 133–146. (doi:10.1016/0169-7439(95)00047-X)
35. Van Benthem MH, Keenan MR. 2004 Fast algorithm for the solution of large-scale non-negativity-constrained least squares problems. *J. Chemom*. **18**, 441–450. (doi:10.1002/cem.889)
36. Kilcrease J, Collins AM, Richins RD, Timlin JA, O'Connell MA. 2013 Multiple microscopic approaches demonstrate linkage between chromoplast architecture and carotenoid composition in diverse *Capsicum annuum* fruit. *Plant J*. **76**, 1074–1083. (doi:10.1111/tpj.12351)
37. Abràmofff MD, Magalhães PJ, Ram SJ. 2005 Image processing with ImageJ Part II. *Biophotonics Int*. **11**, 36–43. (doi:10.1117/1.3589100)
38. Kaufman L, Rousseeuw PJ (eds). 1990 *Finding groups in data*. Hoboken, NJ: John Wiley & Sons, Inc.
39. R Core Team. 2014 *R: a language and environment for statistical computing*. Vienna, Austria: R. See http://www.r-project.org/.
40. Maechler M, Rousseeuw P, Struyf A, Hubert M, Hornik K. 2014 *Cluster: Cluster analysis basics and extensions*. Vienna, Austria: Cran. See https://cran.r-project.org/web/packages/cluster/.
41. Rousseeuw PJ. 1987 Silhouettes: a graphical aid to the interpretation and validation of cluster analysis. *J. Comput. Appl. Math*. **20**, 53–65. (doi:10.1016/0377-0427(87)90125-7)
42. Frederiksen R, Boyer NP, Nickle B, Chakrabarti KS, Koutalos Y, Crouch RK, Oprian D, Cornwall MC. 2012 Low aqueous solubility of 11-cis-retinal limits the rate of pigment formation and dark adaptation in salamander rods. *J. Gen. Physiol*. **139**, 493–505. (doi:10.1085/jgp.201110685)
43. Grothendieck G. 2013 *nls2: Non-linear regression with brute force*. Vienna, Austria: Cran. See http://cran.r-project.org/package=nls2.
44. Goldsmith TH, Butler BK. 2003 The roles of receptor noise and cone oil droplets in the photopic spectral sensitivity of the budgerigar, Melopsittacus undulatus. *J. Comp. Physiol. A, Neuroethol. Sens. Neural Behav. Physiol*. **189**, 135–142. (doi:10.1007/s00359-002-0385-8)
45. Eroglu A, Harrison EH. 2013 Carotenoid metabolism in mammals, including man: formation, occurrence, and function of apocarotenoids. *J. Lipid Res*. **54**, 1719–1730. (doi:10.1194/jlr.R039537)
46. Britton G, Liaaen-Jensen S, Pfander H (eds). 2004 *Carotenoids*. Basle, Switzerland: Springer.
47. Bautista JA, Connors RE, Raju BB, Hiller RG, Sharples FP, Gosztola D, Wasielewski MR, Frank HA. 1999 Excited state properties of peridinin: observation of a solvent dependence of the lowest excited singlet state lifetime and spectral behavior unique among carotenoids. *J. Phys. Chem. B* **103**, 8751–8758. (doi:10.1021/jp9916135)
48. Hart NS, Lisney TJ, Collin SP. 2006 Cone photoreceptor oil droplet pigmentation is affected by ambient light intensity. *J. Exp. Biol*. **209**, 4776–4787. (doi:10.1242/jeb.02568)
49. Bowmaker JK, Heath LA, Wilkie SE, Hunt DM. 1997 Visual pigments and oil droplets from six classes of photoreceptor in the retinas of birds. *Vision Res*. **37**, 2183–2194. (doi:10.1016/S0042-6989(97)00026-6)
50. Coyle BJ, Hart NS, Carleton KL, Borgia G. 2012 Limited variation in visual sensitivity among bowerbird species suggests that there is no link between spectral tuning and variation in display colouration. *J. Exp. Biol*. **215**, 1090–1105. (doi:10.1242/jeb.062224)
51. Toomey MB, McGraw KJ. 2012 Mate choice for a male carotenoid-based ornament is linked to female dietary carotenoid intake and accumulation. *BMC Evol. Biol*. **12**, 3. (doi:10.1186/1471-2148-12-3)
52. Toomey MB, McGraw KJ. 2011 The effects of dietary carotenoid supplementation and retinal carotenoid accumulation on vision-mediated foraging in the house finch. *PLoS ONE* **6**, e21653. (doi:10.1371/journal.pone.0021653)
53. Knott B, Berg ML, Morgan ER, Buchanan KL, Bowmaker JK, Bennett ATD. 2010 Avian retinal oil droplets: dietary manipulation of colour vision? *Proc. R. Soc. B* **277**, 953–962. (doi:10.1098/rspb.2009.1805)
54. Govardovskii VI, Fyhrquist N, Reuter T, Kuzmin DG, Donner K. 2000 In search of the visual pigment template. *Vis. Neurosci*. **17**, 509–528. (doi:10.1017/S0952523800174036)
55. Stavenga DG, Smits RP, Hoenders BJ. 1993 Simple exponential functions describing the absorbance bands of visual pigment spectra. *Vision Res*. **33**, 1011–1017. (doi:10.1016/0042-6989(93)90237-Q)
56. Lind O, Mitkus M, Olsson P, Kelber A. 2014 Ultraviolet vision in birds: the importance of transparent eye media. *Proc. R. Soc. B* **281**, 20132209. (doi:10.1098/rspb.2013.2209)
57. Mandelman T, Sivak JG. 1983 Longitudinal chromatic aberration of the vertebrate eye. *Vision Res*. **23**, 1555–1559. (doi:10.1016/0042-6989(83)90169-4)
58. Lind O, Chavez J, Kelber A. 2014 The contribution of single and double cones to spectral sensitivity in budgerigars during changing light conditions. *J. Comp. Physiol. A. Neuroethol. Sens. Neural Behav. Physiol*. **200**, 197–207. (doi:10.1007/s00359-013-0878-7)